RESEARCH ARTICLE

As(V) removal using biochar produced from an agricultural waste and prediction of removal efficiency using multiple regression analysis

Sneh Lata[1] · Roshan Prabhakar[1] · Asok Adak[2] · Sukha Ranjan Samadder[1]

Abstract

Arsenic contamination in drinking water is a matter of concern for many countries. An efficient and low-cost solution for this hazard is essentially needed on urgent basis. Therefore, in this study, banana pith (an agricultural waste) was used for biochar production and later it was modified with iron and applied for arsenic adsorption from aqueous solution. Produced biochar was characterized for proximate, ultimate, and surface analyses. Interestingly, after iron impregnation, the surface area of biochar increased (31.59 m^2/g) by nearly 8 times. Morphological analysis showed that iron particles firmly held within the pores after impregnation. Arsenate (As(V)) adsorption behavior of iron-impregnated banana pith biochar was evaluated through a batch study by considering various parameters like dose, concentration, pH, temperature, and competing anions. Compared to impregnated biochar, raw biomass and its biochar showed a lesser affinity for arsenate in aqueous solution. The adsorption isotherm of As(V) on banana pith biochar was covered in the temperature range of 298 to 318 K, and kinetic data of adsorption was experimentally generated at 298 K. Langmuir model for the sorption isotherms and pseudo-second-order kinetic model for the sorption kinetics represented the experimental data. The thermodynamic study showed negative Gibb's free energy (− 46.88 kJ/mol at 298 K, − 48.58 kJ/mol at 308 K, − 50.73 kJ/mol at 318 K) that suggested spontaneity of the adsorption process. Negative enthalpy ($\Delta H° = − 10.55$ kJ/mol) showed exothermic nature of adsorption of arsenic, while negative entropy ($\Delta S° = 0.123$ kJ/mol.K) suggested enthalpy-driven adsorption process. Mechanism of arsenic adsorption onto iron-impregnated banana pith biochar has also been discussed in detail. Based on the experimental observation, a predictive model for arsenate removal has been developed in this study. The findings of the present study elucidated that iron-impregnated banana pith biochar can be used as a low-cost adsorbing material for As(V) from aqueous solutions.

Keywords Arsenic · Agrowaste · Banana pith biochar · Surface modification · MLR modeling

✉ Sukha Ranjan Samadder
samadder@iitism.ac.in; sukh_samadder@yahoo.co.in

1 Department of Environmental Science & Engineering, Indian Institute of Technology (Indian School of Mines), Dhanbad 826004, India

2 Department of Civil Engineering, Indian Institute of Engineering Science and Technology, Howrah, Shibpur, India

Introduction

Contamination of groundwater by the occurrence of different heavy metals and metalloids is a global concern today (Yonesian et al. 2012; Qasemi et al. 2019). Among the several contaminants in water, arsenic (As) has got the spotlight because of its worldwide presence and several detrimental effects on the biosphere (Dehghani et al. 2017a). Approximately, throughout the world, 1.8 billion people are affected by this groundwater menace (WHO 2014). On a global scale, Asian countries like India and Bangladesh share a major proportion of arsenic contamination of groundwater (Roy et al. 2015). The natural geological condition and anthropogenic actions like the application of pesticides, wood preservatives, and mining activities are the major causes of arsenic leaching into groundwater (Mudhoo et al. 2011). The exact releasing mechanism of

arsenic is still debatable among researchers. However, reductive dissolution of arsenopyrite under the anoxic condition and also the oxidation of arsenic-bearing minerals are generally believed to be the causes of leaching (Siddiqui and Chaudhry 2017). Generally, in groundwater, inorganic arsenic species like trivalent arsenite and pentavalent arsenate are the majorly found arsenic anions. Their existence in groundwater is subjected to redox potential and pH condition (Thanh et al. 2016). Drinking arsenic-laden water can cause cancers in different vital organs. It can also cause neurological illnesses, cardiovascular and cerebrovascular diseases, diabetes mellitus, and adverse reproductive effects (Carlin et al. 2015). The International Agency for Cancer Research (IARC) has categorized arsenic as a class I carcinogen (Hughes et al. 2000). Considering the associated health risks, stern guideline has been declared to suggest the maximum permissible limit as 10 ppb in drinking water. In order to comply with the guidelines, membrane separation, coagulation, ion exchange, and adsorption are the commonly used methods for removal of arsenic (Crittenden and Harza 2005). Adsorption of arsenic on adsorptive media has been found a more feasible process because of less environmental impacts than other methods and comparatively less requirement of capital, energy, and chemicals (Mohan and Pittman 2007). In this regard, the number of conventional adsorbents of natural and synthetic origin such as sand, fly ash, plant biomass, activated carbon, and activated alumina have been used to treat arsenic from groundwater (Pintor et al. 2018; Montero et al. 2018). However, most of the conventional adsorbents have irregular pore structures and low specific surface areas, leading to low adsorption capacities. Lack of selectivity, relatively weak interactions with metallic ions, and regeneration difficulties can also confine the ability of these sorbents in lowering arsenic concentrations below permissible limits (Samiey et al. 2014). Apart from the said drawbacks, these are of high cost that have stalled their applications. Selection of suitable adsorbent is key to the success of adsorption practices. Therefore, the need of the hour is to find an effective and eco-friendly sorbent with higher removal of arsenic from aqueous solutions. In recent years, biochar (BC), an alternative to widely used adsorbent (activated carbon), has been utilized for different contaminant removal from water and wastewater (Mohan et al. 2014; Rizwan et al. 2016). It has almost replaced the conventional activated carbon and several other adsorbents due to its unique features like low-cost and eco-friendly nature (Lata and Samadder 2016). Selection of feedstock and pyrolysis condition determines the property of biochar. Generally, plant-based materials are used as feed stock for biochar production. Nowadays, the conversion of organic waste into worthy biochar products is seemingly a viable option for the disposal of these wastes. Therefore, banana pith was used in this study, which is a pseudostem and usually thrown away after harvesting the banana fruit. It contains a number of electrolytes. Therefore, this agricultural

waste was chosen as feed stock for the production of biochar, as it is easily available and of no economic value. Further, this will serve as an adsorbent for arsenic removal. Along with the surface area of BC, its surface chemistry also plays a prominent role in arsenic removal. In general, biochar is carbon-rich material, which is produced by the process of pyrolysis. Being carbonaceous in nature, it carries a net negative charge on the surface, which is good for the removal of cationic pollutants and heavy metals (Zhou et al. 2017). Due to negatively charged surface, biochar had shown repelling behavior for anions like arsenate and phosphate (Mukherjee et al. 2011; Tang et al. 2013). These days, surface modification of biochar came into the limelight for improvement in adsorption efficiency (Tan et al. 2016). For instance, chitosan-modified biochar was used for chromium removal (Zhang et al. 2015); biochar impregnated with Cu(II) was applied for doxycycline hydrochloride removal from water (Liu et al. 2017). It is well known that the iron hydroxide poses a good adsorbing capacity for arsenic anions by ligand formations (Hering et al. 1996; Montero et al. 2018). However, it was also seen that when iron particles are used individually, aggregates formed in aqueous solutions that intensely decrease the surface area resulting in less adsorption capacity and eventually increase the cost (Vindedahl et al. 2016). Thus, to enhance the adsorbing power of biochar and to overcome the problems in using iron as an adsorbent, surface modification of biochar using iron salt is very imperative and may produce desired results. In the present work also, after synthesizing the biochar from the banana pith, it was impregnated with iron salt. Usually, removal of neutral As(III) from drinking water needs dissociation in an anionic form that occurs above pH 9 or it requires oxidation into As(V). Increase in pH makes the water unfit for drinking; hence, oxidation of As(III) into As(V) prior to removal from drinking water was found the best-reported method (Sorlini and Gialdini 2010). Therefore, in the present study, only As(V) (arsenate) was chosen as target anion to be removed. Overall, the goal of this work was to find an easy-to-use and low-cost waste-based adsorbent for removing As(V) from water solutions. Specifically, the synthesized biochar material was characterized by knowing the surface characteristics. Further, the removal efficiency of this biochar was evaluated by considering the different influencing parameters like dose, time, concentration, pH, and temperature. Finally, using experimental data, a model was developed to forecast the removal efficiency.

Materials and methods

Materials

Analytical grade chemicals were used as received. All the solutions during the study were made using type II deionized water (18 MΩ cm). Glasswares were cleaned and sterilized in

a hot air oven and rinsed with deionized water before its use. One thousand milligrams per liter of stock solution concentration of As(V) ($NaH_2AsO_4 \cdot 7H_2O$, Merck, Germany) was made and working solutions were made with appropriate dilution. pH of the working solutions was accustomed using 0.1 N NaOH or HCl as needed.

Methods

Banana Pith biochar preparation

Banana pseudo stems were collected from Lucknow, India. First of all, layers of pseudo stem were peeled off to obtain central 4–5-cm core of the pith. Then the piths obtained were washed with running tap water and cut into small pieces. These pieces of banana pith were then boiled for 15 min to remove the mucus content. Further, these were sun-dried for 10–15 days for removal of moisture, then were grinded into coarser particle size. These coarser particles were pyrolyzed at 200 °C for 4 h using muffle furnace and, further, the temperature was raised up to 400 °C for 15 min. The prepared banana pith biochar was sieved through 125-μm sieve and was retained on 75-μm sieve.

Surface modification of biochar

The surface modification of as-prepared banana pith biochar (BPB) was carried out with ferric nitrate nonahydrate. During the modification course, to 100 mL of 250 g/L ferric nitrate nonahydrate solution, 4 g of banana pith was added. The solution containing iron and BPB was stirred at 500 rpm for 6 h. For proper iron distribution and its subsequent diffusion into the pores of banana pith biochar structure, the solution was left for 3 days in ambient condition (Cope et al. 2014). After 3 days, the solution was filtered using filter paper (Whatman no. 42) and obtained iron-impregnated banana pith biochar (FeBPB) was air-dried for 24 h. Further, it was cleaned with deionized water and oven-dried at 80 °C for 8 h. Finally, the modified iron-impregnated banana pith biochar was kept in an airtight jar for its further use as an adsorbent for As(V) removal.

Adsorbent characterization

Surface morphology of the adsorbent was determined using field-emission scanning electron microscopy (FESEM, Supra 55) which was employed for determining the surface morphology. Quantachrome Autosorb-1 surface area analyzer was employed to measure samples specific surface area. The determination of the pH_{zpc} of the adsorbents was performed by the method explained by Mohan et al. (2012). To determine the pH_{zpc} of adsorbent, different doses of adsorbent (0.5, 1, 1.5, 2, 2.5 g/l) were added into deionized water and were adjusted to diverse pH values (3.5 to 12.5). The samples were stirred for 48 h. pH of each sample at equilibrium condition was measured when the adsorbent settled. The pH_{ZPC} was estimated when the pH of the water did not change on contact with the samples. Fourier transform infrared (FTIR) spectroscopy (Cary 660, Agilent Technology, USA) was used to analyze different functional groups present on the adsorbent surface. Phase analysis of iron and adsorbed arsenic was done using X-ray diffraction (XRD, Ultima IV, Rigaku, Japan). X-ray photo electron spectroscopy (XPS) (PHI 5000 Versa Probe II, ULVAC–PHI, INC, Japan) with a microfocused (100 μm, 25 W, 15KV) monochromatic Al-Kα source (hν = 1486.6 eV) was used to measure the surface element composition and speciation. Typical vacuum pressure in the analysis chamber during the measurements was in the order of 10^{-10} torr. Proximate analysis was performed using muffle furnace (NEC BRAND, India) using the procedures of ASTM standards and ultimate analysis was performed using Elemental Analyzer (EURO EA).

Sorption study

Batch optimization studies were executed to know the impact of different parameters like contact time (10–300 min), adsorbent dose (1–6 g/L), initial As(V) concentration (50–500 μg/L), and pH (3.5–10.5) on As(V) removal using iron-impregnated banana pith biochar. The study was done by changing one parameter at a time while others were kept constant. The reaction mixture was agitated in an incubator shaker at 172 ± 2 rpm for 8 h to achieve the equilibrium. The equilibrium was achieved after 8 h, then the solution was filtered using filter paper (Whatman no. 42). Isotherm and kinetic studies have also been conducted to determine the behavior of adsorption for removal of As(V). The isotherm study was executed at three different temperatures (298, 308, and 318 K) by varying the initial concentrations in a wide range (50–500 μg/L). This solution with varying concentration and pH of 6.5 was supplemented by a fixed dose of 2.5 g/L and contacted for 120 min. Similarly, kinetic studies were investigated at pH value of 6.5 with a fixed arsenate concentration (100 μg/L) and dose (2.5 g/L); solutions were agitated for a different time interval ranging from 10 to 150 min. Likewise, the thermodynamic studies were performed by conducting the experiments at different temperatures (298 K to 318 K). The influence of the presence of diverse anions on the adsorption arsenate, for instance, nitrate, phosphate, silicate, and sulfate, was observed for the current study. During adsorption studies, samples were withdrawn at a predetermined time and the remaining As(V) concentration in the filtrate was determined using an atomic absorption spectrophotometer (Avanta PM, GBC, Australia). Each experiment was performed in triplicate and the average values have been reported. The efficiency of the arsenic hydride generation process depends strongly on the valence state

of the arsenic ions present. As(III) shows approximately twice the sensitivity of As(V). Therefore, for detection of As(V) present in solution, the sample of As(V) was reduced with HCl (with 20% v/v of total sample size) and KI solution with concentration of 200 mg/L.

The amount of arsenic adsorbed at equilibrium, i.e., q_e (μg/g) was calculated using Eq. (1) (Dehghani et al. 2018a).

$$q_e = \frac{V(C_0 - C_e)}{M} \tag{1}$$

Percentage arsenic removal (R) was calculated using Eq. (2);

$$R\ (\%) = \frac{(C_0 - C_e)}{C_0} \times 100 \tag{2}$$

where C_0 represents initial As(V) concentration and C_e signifies As(V) concentrations in equilibrium condition. Both symbols have unit of micrograms per liter. V is the volume (L) and M is the amount (g) FeBPB used.

Prediction modeling (multiple linear regression analysis)

The data obtained after adsorption studies were used for prediction modeling. In this light, multiple linear regression modeling (MLR) approach was identified and applied to experimental observations. Generally, in MLR modeling, coefficients for several independent variables are found to establish its relation and effects on dependent variables. The mathematical expression of this model for given n observations is stated by Eq. (3) (Kumar and Samadder 2017).

$$Y = \beta_0 + \beta_1 X_1 + \beta_2 X_2 + \beta_3 X_3 + \ldots \ldots \beta_n X_n + \varepsilon \tag{3}$$

where Y is the predicted (dependent) variable, β_0 represents the value of Y-intercept, $\beta(1\ldots n)$ are the coefficients of regression, $X(1\ldots n)$ are the predictors for independent variables, and ε shows stochastic error of the regression. In the present study, SPSS 21.0 was used to see the collective effects of various independent factors like concentration, dose, temperature, contact time, and pH on a dependent variable, i.e., removal efficiency by MLR analysis. Separate experimental observations have been used for model development and its validation.

Results and discussion

Characterization study of FeBPB

Surface morphology plays the main role in understanding the interactions between adsorbent and adsorbate. FESEM images of banana pith biochar (BPB) and iron-impregnated banana pith biochar (FeBPB) are shown in Fig. 1. These figures clearly demonstrate that adsorbent surface became more porous after converting it into biochar. After iron impregnation, pores were filled with iron and surface became rough. Specific surface areas were found as 4.331 m²/g for banana pith biochar (BPB) and 31.59 m²/g for FeBPB. The surface area should have decreased, but the surface area of BPB increased by 8 times after iron impregnation. This is due to the fact that the diffusion of iron was completed as the biochar and the iron-containing solution was left for three days after shaking. Biochar-imbibed water opened the pores or adsorption sites available at biochar surface and attached the iron over the opened pores. The deviation in the pH in equilibrium condition at changed adsorbent doses of FeBPB is shown in Fig. 2. pH_{zpc} of FeBPB was found as 9.5 indicating that below this pH, adsorbent surface had positive charge that enhanced uptake of anions. Hence, As(V) ions were effectively removed even up to pH 7.5. Fourier transform infrared (FTIR) analysis of iron-impregnated banana pith biochar before and after As(V) adsorption revealed the presence of several peaks in IR spectra (Fig. 3). The peaks ranged between 2850–2960 cm^{-1} and 1366–1382 cm^{-1} ascribed to alkane. Presence of peaks in FeBPB and FeAsBPB at 2353.41 cm^{-1} showed its

Fig. 1 FESEM images of **a** banana pith biochar (BPB) and **b** iron-impregnated banana pith biochar (FeBPB)
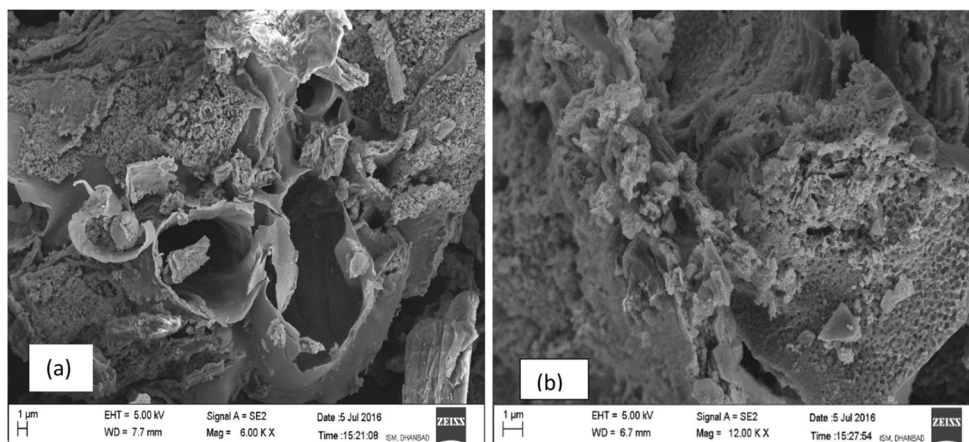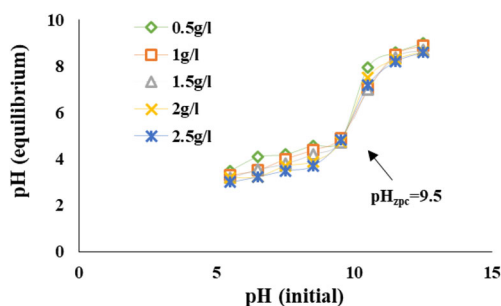
Fig. 2 Zero point charge (pHzpc) determination of iron-impregnated banana pith biochar (FeBPB)

Fig. 4 XRD analysis of RBP, BPB, FeBPB, and FeAsBPB

insignificant role in biochar preparation and As(V) adsorption. Peak at wave number that ranged from 3386.29 to 3383.65 cm^{-1} showed presence of –OH group. Alteration in peak from 3386.29 to 3383.65 cm^{-1} indicated contribution of hydroxyl group in adsorption of arsenate. There was another shift in peak from wave number 1027.81 to 1082.69 cm^{-1} (in FeBPB and FeAsBPB) and the peak range is ascribed for carbonyl group (C=O). This suggested carbonyl group contributed in adsorption of arsenate. A very small sharp peak at 690 cm^{-1} was also found in FeAsBPB that ascribed to As–O stretching (Jia et al. 2007). X-ray diffraction (XRD) exploration of the raw banana pith and banana pith biochar indicated the presence of crystalline calcite (C) and quartz (Q), but iron-impregnated banana pith biochar showed amorphous structure (Fig. 4). The amorphous iron hydroxides/oxides reduced the negative charge on the biochar surface that supported the increase in As(V) adsorption. Therefore, it can be concluded that non-crystalline iron hydroxide/oxide surface had significant contribution in As(V) adsorption. The peaks (*d*-values) were coordinated, with X'Pert High Score Plus files and the crystalline phases were identified. X-ray diffraction (XRD) spectra specified the presence of crystalline calcite and quartz in raw banana pith (RBP) and BPB. In FeBPB, there were small peaks of iron at two theta values of 36.8, 35, and 33 (ICDDPDF No. 01-081-0464) that indicated the presence of iron in hydroxide phase. In FeAsBPB, no sharp peak was
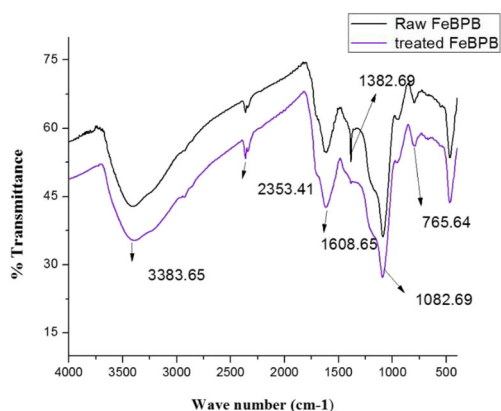
observed that indicated As(V) adsorption was in amorphous form. The XPS spectra, obtained for FeBPB (Fe_{2p}, O_{1s}, O_{2p}, C_{1s}) and FeAsBPB (Fe_{2p}, O_{1s}, O_{2p}, C_{1s}, As_{3d}), are displayed in Fig. 5. The peak of O_{1s} at 531.3 eV (in FeBPB and FeAsBPB) is the most intense and is ascribed to –OH of hydrous iron oxides such as FeOOH. Presence of peak at 25.8 eV of O_{2s} showed oxygen is present in the form of water (in FeBPB and FeAsBPB). The C_{1s} spectrum showed peak at a binding energy of 284.6 eV (FeBPB and FeAsBPB). This peak is endorsed to the C–C and C–H groups in both cases. The Fe_{2p} and As_{3d} spectrum showed complex forms of different corresponding species that were deconvoluted using the software XPS Peak-Fit 4.1 (Fig. S1, S2). The Fe_{2p} spectrum of FeBPB and FeAsBPB exhibited peaks at 711.2 eV and 725.8 eV for $Fe_{2p3/2}$ and $Fe_{2p1/2}$ individually, which are credited to ferric compounds such as ferric oxide and oxyhydroxide (Fe_2O_3, FeOOH). The 3d spectrum of FeAsBPB exhibited peak at 45.5 eV (Na_2HAsO_4). Fe_{2p} orbital binding energies were reported as 724.3 eV (FeOOH), and 709.4 eV $[Fe(C_6H_4(As(CH_3)_2)_2)](ClO_4)_3$. Binding energies of As_{3d} have been reported as 41.5 eV, 44.2 eV, and 45.5 eV for As(0) and As(III) in $NaAsO_2$ and for As(V) in Na_2HAsO_4 respectively (Fig. S3). In the present study, there was a small peak at 45.5 eV for As_{3d}, but there was no peak of As_{3d} binding energy of 44.2 eV, i.e., ascribed to As(III); this implies that arsenic was adsorbed as As(V) only and there was no conversion of As(V) into As(III). Binding energies of the elements present in the adsorbent before and after adsorption of As(V) were matched with NIST database that indicated the presence of iron in + 3 and arsenic in + 5 oxidation states. The results of the proximate analysis revealed that there was very less ash content in RBP, because that was not pyrolyzed (Table 1). The ash content in BPB prepared after pyrolysis was less than 50% that indicated it can be termed as biochar as per guidelines for specifications of biochars by the International Biochar Initiative. Fixed carbon increased after converting the raw banana pith into biochar. This indicated the preparation of biochar assisted in carbon storage in biochar. In the ultimate analysis, the content of all the elements increased except oxygen after pyrolysis (BPB), because all the elements

Fig. 3 FTIR analysis of raw FeBPB and arsenic loaded (treated) FeBPB

Fig. 5 XPS analysis of **a** FeBPB and **b** FeAsBPB
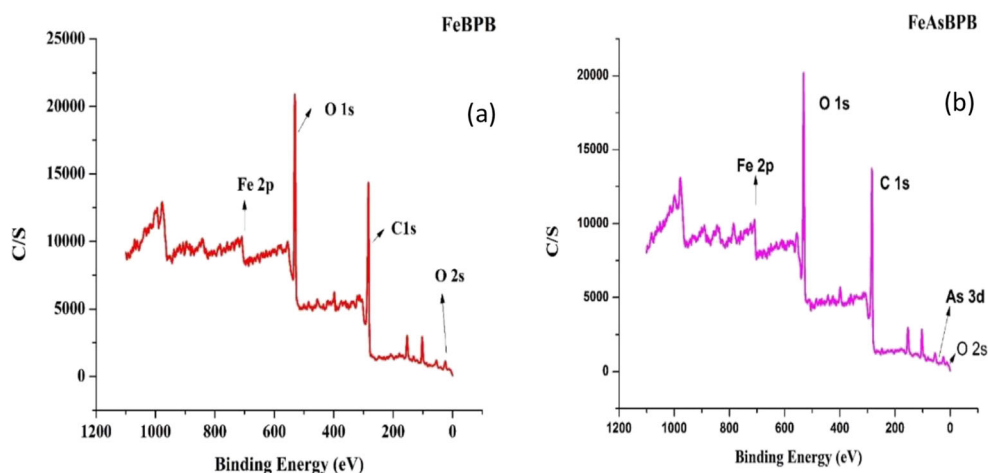
concentrated after pyrolysis, while oxygen was used in pyrolysis and in carbon storage.

Comparative removal efficiency of raw banana pith biomass, banana pith biochar, and iron-impregnated banana pith biochar

Comparison of removal efficiency of RBP, BPB, and FeBPB was performed with a fixed amount of arsenate concentration (100 µg/L). Adsorbent dose was varied from 1.5 to 25 g/L. Removal efficiency of RBP was observed from 1.64 to 42.66% (Fig. 6). While for BPB, it ranged from 12.59 to 67.1%. RBP and BPB had very poor removal efficiency for As(V) in whole dose regime. In the case of FeBPB, 100% removal was achieved at a very low adsorbent dose (2.5 g/L). It was evident from the results that iron on biochar surface produced a synergistic effect on removal. The reason could be the positive surface charge development and increase in surface area, which has already been elaborated in the

Table 1 Results of the proximate and ultimate analysis of RBP and BPB

Properties	RBP	BPB	Standard method
Proximate analysis			
Volatile matter (%)	42.63	14.8	ASTM D5832−98
Ash (%)	12.02	37.4	ASTM D2866−11
Moisture (%)	7.54	1.06	ASTM D2867−09
Fixed carbon (%)	31.71	47.8	By difference
Ultimate analysis			
C (%)	38.635	49.40	Elemental analyzer
H (%)	1.805	3.266	
N (%)	1.257	3.201	
S (%)	0.25	0.285	
O (%)	57.03	45.14	By difference

previous section. The adsorbent for the water treatment system should be capable of removing the contaminant to the desirable level. Thus, considering the removal efficiencies, further studies were carried out using iron-impregnated banana pith biochar (FeBPB).

Effects of the individual parameter on removal efficiency

Contact time

For developing a feasible and large-scale adsorption-based treatment system, estimation and optimization of contact time are of utmost importance. Thus, for the present study, in the 100-mL solution of 100 µg/L As(v) concentration, a fixed amount of FeBPB (0.25 g) was added and shaken (170 rpm) for different time periods ranging from 10–300 min. pH of the solution was maintained at 6.5 and adsorption experiment was performed at 25 °C. Results of contact time optimization showed that the percentage As(V) removal augmented with increase in contact time until all its active sites were occupied and there was no more adsorption of As(V) (Fig. 7a). From the results, it was witnessed that the remaining arsenate
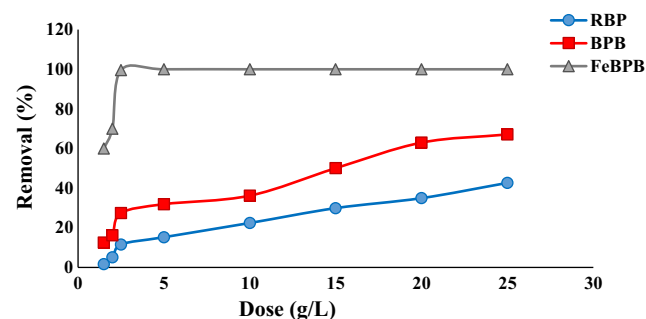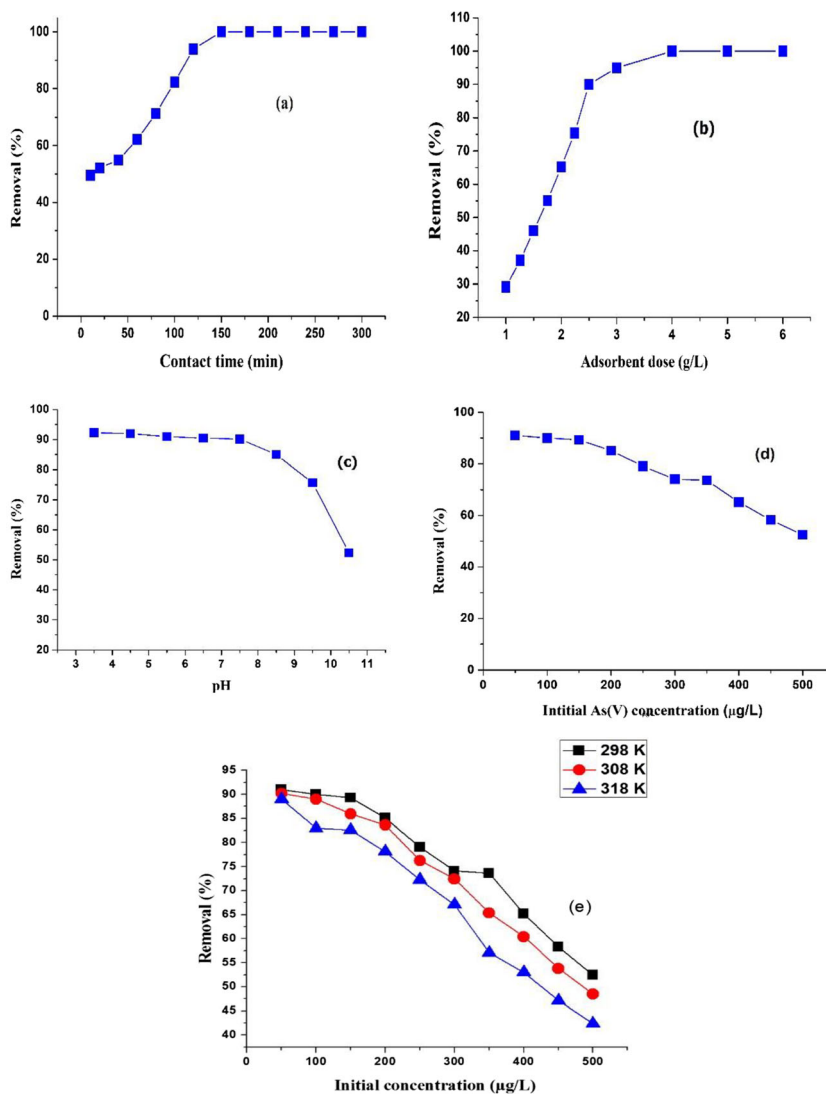

Fig. 6 Comparison in removal efficiency of As(V) using raw and modified banana pith biochar

Fig. 7 Effects of individual parameter on As(V) removal of **a** contact time, **b** initial concentration, **c** adsorbent dose, **d** pH, and **e** temperature

concentration at contact time of 120 min (2 h) was found as 8.95 μg/L, which is well below the recommended concentration. At this contact time, very high removal (91.05%) was observed. Therefore, considering the achievement of safe limit of residual arsenic concentration, contact time of 2 h was chosen for further study.

Adsorbent dose

In order to define the economy of the treatment system, optimization of the adsorbent dose is a very essential step in the adsorption process. This optimization was done with a solution having a concentration of 100 μg/L and pH of 6.5. Adsorbent dose was varied from 1 to 6 g/L. Sorption experiment was performed at the temperature of 25 °C. The influence of adsorbent dose on As(V) adsorption is displayed in Fig. 7 b. The adsorption of As(V) got enhanced with the increase in adsorbent dose. As(V) adsorption onto FeBPB

showed that adsorption became constant above 2.5 g/L of FeBPB dosage. The adsorbent dose of FeBPB above 2.5 g/L indicated a constant nature of the graph indicated that solute was used completely. Further increase in adsorbent dose had not shown any substantial increase in removal. This might be due to the attachment of almost all As(V) ions on the adsorbent sites or attaining the equilibrium.

pH

pH of a solution plays a vital role for process of arsenic adsorption, as it considerably affects the adsorbent surface charge and speciation. Therefore, it is of prime importance to find a suitable and optimal pH for the efficient removal of As(V). In the present study, pH optimization study was carried out with 100 μg/L arsenate concentration and 2.5 g/L of adsorbent dose. Solution pH was varied from 3.5 to 10.5. Other parameters were kept the same as discussed in previous

optimization studies. More than 90% of removal was seen up to pH 7.5, but percentage As(V) removal decreased when pH exceeded 7 (Fig. 7c). Increase in pH made the adsorbent surface negatively charged that caused repulsion between the same charged species. Therefore, there was a decline in percentage of removal that was detected with an increase in pH. This specific behavior in removal pattern can be elucidated in terms of zero point charge value of FeBPB. The pHzpc value of FeBPB was found as 9.5. At pH < pHzpc, the FeBPB surface was positively charged due to protonation, whereas at pH > pHzpc, surface developed a negative charge, which caused a decline in removal with rise in solution pH (Prabhakar and Samadder 2018). Besides, the hydroxyl ion concentration also got augmented with increase in pH that also provided a competition adsorption sites (Patra et al. 2012).

Initial As(V) concentration

Concentration of As(V) is one of the prime adsorption governing aspects, as it is responsible for decreasing the mass transfer resistance between adsorbate and adsorbent. Hence, its influence on the efficiency of removal was carried out. Range of concentrations varying from 50 to 500 µg/L was used. One hundred milliliters of the solution of the mentioned concentrations having pH 6.5 was made and to this, a fixed amount (0.25gm) of FeBPB was added. The samples were agitated in an incubator shaker (25 °C) at 170 rpm for 120 min. From the experimental data, it was established that the removal efficiency depends on the concentration of arsenate. The percentage As(V) removal got decreased with rising concentration. 2.5 g/L of FeBPB dose was found effective to bring the As(V) concentration below 10 µg/L up to the concentration of 150 µg/L (Fig. 7d). This happened due to more number of arsenate ions contending for the accessible sites for adsorption in the biochar. Similarly, at higher concentrations, sites of adsorption were limited.

Temperature

Temperature has always been considered the most effective parameter for adsorption processes. Study of this effect becomes necessary, because of global variation in temperature, which certainly provides an assessment tool for its wide-scale application. To know the effect of temperature, experiments were executed at three different temperatures (298–318 K). The As(V) solutions of different concentrations (50–500 µg/L) along with other optimized parameters (dose, 2.5 g/L; pH, 6.5; temp., 25 °C) were shaken. From Fig. 7 e, it was perceived that adsorption kept on decreasing for all studied concentrations by changing the experimental temperature from 298 to 318 K. The removal performance was highest at 298 K. The elevated temperature of solution has been observed to be less effective for the enhancement in removal

efficiency. The results preliminary reflected the exothermic nature of adsorption. With this observation, it can be hypothesized that with an increase in temperature, surface might have attained higher energy which caused the escaping of adsorbed arsenate ions into bulk solution. The observations of temperature-related study inferred the appropriateness of this adsorbent approach in natural condition.

Adsorption isotherm

Isotherm modeling can effectively help in designing the adsorption-based treatment system. It can also assist in illustrating the mechanism and applicability of the adsorption process. Langmuir and Freundlich are the two well-known and applicable isotherm models for single solute system. It is always advisable and advantageous to use nonlinear equations of these models; as with linearization, biasness occurs by variation in its error structures. Thus, in the current work, data were modeled and assessed using nonlinear form of Langmuir and Freundlich isotherm models as presented in Eqs. (4) and (5) correspondingly (Velazquez-Jimenez et al. 2018). Furthermore, the fitness of models was evaluated not only as a function of R^2 but also considered error functions like sum of square error (S.S.E) and chi-square (χ^2) which are represented by Eqs. (6) and (7) respectively.

$$Q_e = \frac{Q_m K_L C_e}{1 + K_L C_e} \quad (4)$$

$$Q_e = K_f C_e^{1/n} \quad (5)$$

$$\text{S.S.E} = \sum_{i=1}^{n} \left(q_{e.calc} - q_{e.exp} \right)_i^2 \quad (6)$$

$$\chi^2 = \sum_{i=1}^{n} \frac{\left(q_{ecalc} - q_{eexp} \right)^2}{q_{eexp}} \quad (7)$$

In these equations, Q_e and C_e have the usual definitions as described earlier. Q_m (µg/g) represents the Langmuir maximum uptake or adsorption capacity and K_L (L/µg) is the Langmuir adsorption constant. q_{ecalc} and $q_{e\,exp}$ show the model calculated and experimental adsorption capacity correspondingly. As per the assumptions of Langmuir isotherm model, adsorbent surface contains active sites of uniform energy which facilitates the monolayer adsorption process (Dehghani et al. 2017b; Khosravi et al. 2018). After occupying the designated active sites, the adsorbing molecules cannot interact with neighboring molecules (Allen et al. 2004); beyond this monolayer coverage, no further adsorption is allowed and the surface saturates, which provides the maximum adsorption capacity. The constants for Langmuir model were obtained from Fig. 8. Table 2 presents the observed values of Langmuir isotherm parameters at three different temperatures. The K_L values indicated the sorption energy,
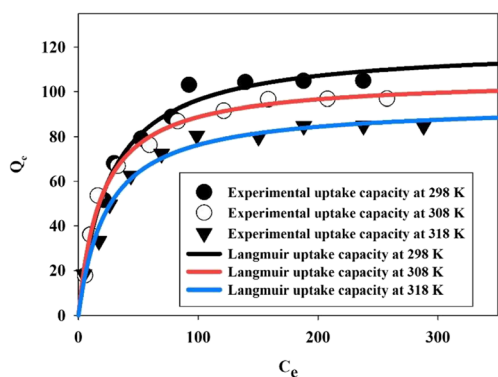
Fig. 8 Nonlinear Langmuir adsorption isotherm plot for As(V) adsorption using FeBPB

Fig. 9 Nonlinear Freundlich adsorption isotherm plot for As(V) adsorption using FeBPB

which changed with the temperature. The K_L values at 298, 308, and 318 K were observed as 0.051, 0.041, and 0.039 L/μg correspondingly. The values of K_L showed a decent binding of arsenate at every temperature. At 298 K, adsorption capacity (Q_m) was calculated as 120.91 μg/g, while at 308 and 318 K, these were found as 105.91 and 94.53 μg/g congruently. The decrease in Q_m and K_L values evince the exothermic behavior of adsorption. At 298 K, the χ^2 and S.S.E were found as 7.56 and 438.28.

Similarly, Freundlich isotherm helps in understanding the multilayer adsorption process occurring on heterogeneous surfaces. The graph was plotted as per its nonlinear expression (Eq. 5) and the results are depicted in Fig. 9. Table 2 comprises the parametric values of this model. The values of "n" were found between 3.11 and 3.58. In general, the "n" values in the range of 1–10 endorse a very good sorption intensity and also provide the nature of adsorption to be satisfactory (Khan et al. 2013). Compared to Freundlich isotherm, Langmuir provided lower values of error functions at all the investigated temperatures (Table 2). Also, by observing the R^2 values of both the isotherm models (Table 2), it can be understood that Langmuir
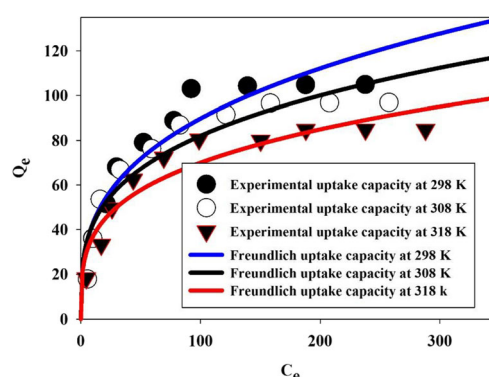
isotherm model was found to represent the experimental data. Maximum adsorption capacity of FeBPB at 298 K was observed as 120.91 μg/g. The Langmuir maximum uptake capacity was found higher than some of the adsorbents cited in the literature for As(V) removal (Table 3). It is a well-known fact that surface area and the initial adsorbate concentration are defining factors for uptake capacities of an adsorbent. In many of the previous studies, arsenic concentration has been taken in the parts per million range that resulted in the high values of adsorption capacities. However, the reported initial concentration range in those studies does not characterize the naturally occurring arsenic concentration range. Selected arsenic concentration range in this study mimics and presents an average value found in similar studies (Ghosh et al. 2019). This study identified FeBPB's potential as a very efficient and cheap adsorbent for removing As(V) under natural circumstances.

Kinetic study

The information on the rate of As(V) removal is essentially required for designing the adsorber for any useful application. Therefore, experiment for kinetics was conducted to understand the mechanism and characteristics of As(V) adsorption using FeBPB. Therefore, pseudo-first-order kinetic model proposed by Lagergren (Lagergren 1898) and pseudo-second-order kinetics of Ho (Ho 1995) was applied to the experimental data. Pseudo-first-order model is centered on the solid capacity and pseudo-second-order model takes solid-phase adsorption into account for revealing the mechanism. Nonlinear equations of these models are expressed by Eqs. (8) and (9).

$$q_t = q_e\left(1 - e^{-k_1 t}\right) \tag{8}$$

$$q_t = \frac{k_2 q_e^2 t}{1 + k_2 q_e t} \tag{9}$$

where q_e has already been discussed and q_t is the uptake capacity at a defined time. k_1 and k_2 are the respective rate
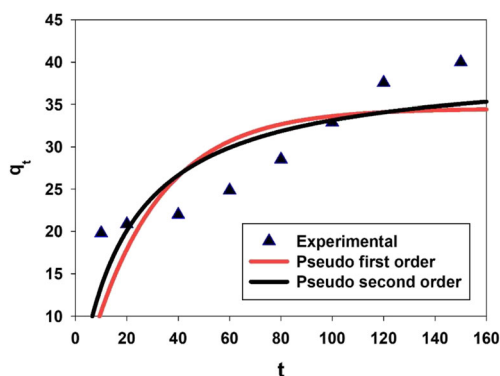
Table 2 Adsorption isotherm parameters for As(V) removal by FeBPB

Isotherm models	Temperature (K)		
Langmuir isotherm	298 K	308 K	318 K
Q_m (μg/g)	120.91	105.91	94.53
K_L (L/μg)	0.051	0.041	0.039
R^2	0.983	0.986	0.981
χ^2	7.56	5.54	2.27
S.S.E	438.28	266.43	92.22
Freundlich isotherm			
K_f {(μg/g)/(μg/L)$^{1/n}$}	20.41	21.88	19.42
n	3.11	3.48	3.59
R^2	0.893	0.897	0.888
χ^2	16.48	14.50	11.47
S.S.E	963.44	721.79	573.73

Table 3 Adsorption capacities of various adsorbents used for As(V) removal

Adsorbent	Maximum adsorption capacity (µg/g)	Reference
Bagasse fly ash	19.76	Ali et al. (2014)
Chemically modified wheat straw	112.3	Ebrahimi et al. (2013)
Industrial waste-based magnetite	120	Randhawa et al. (2014)
Manganese oxide pillared clays	26.17	Mishra and Mahato (2016)
Iron oxide pillared clays	25.73	Mishra and Mahato (2016)
Iron-impregnated banana pith biochar	120.91	Present work

constants for the models. Nonlinear plot of "t" vs "q" yielded the values of kinetic constants (Fig. 10) and is reported in the table. Values of k_1 and k_2 were found as 0.0365 min^{-1} and 19.41×10^{-2} g µg^{-1} min^{-1}. From Table 4, it may be observed that the R^2 value for pseudo-first-order kinetic was lower than the pseudo-second-order kinetics. Also, the calculated uptake capacity ($q_{e\ calc}$) using pseudo first order shows 13.65% deviation with the experimental value ($q_{e\ exp}$). Therefore, pseudo first order was not found valid for the As(V) adsorption on FeBPB. Conversely, in the case of pseudo second order, experimental adsorption capacity matched well with calculated uptake capacity; and the values of error function like χ^2 (0.004) and S.S.E (0.16) were found lower than the pseudo-first-order kinetics. It was interesting to see that nonlinear fitting gave lower value of R^2 than the linear fitting. However, the error function values were found higher for the linear fitting than the nonlinear fitting (Figs S4 a and b; Table S1). The $q_{e\ calc}$ values of pseudo first and second order showed a huge deviation of 13.65% and 21.6% with the $q_{e\ exp}$. It can be seen that in both the method of fitting, only the pseudo-second-order kinetic model was followed and described the experimental data. Similar findings have been reported for the multi-metal removal using waste chestnut shell (Vázquez et al. 2012). The results of this study clearly evince that R^2 cannot be a sole parameter for the fitness of the model. Therefore, it is advisable to use kinetic models in its pure and nonlinear form.

Abovementioned models could not explain the rate-determining step for As(V) adsorption using FeBPB. Therefore, the intraparticle diffusion model was employed to experimental data in order to know the mechanism involved during the physical transfer of arsenate ions on FeBPB. This model is expressed by Eq. (10) (Weber and Morris 1963).

$$q_t = k_{id}t^{0.5} + C \qquad (10)$$

where k_{id} ($_{µgg}^{-1}{}_{min}^{-0.5}$) is the intraparticle diffusion constant and C is the intercept linked to the boundary layer thickness. Plot q_t vs $t^{0.5}$ gave the value of constants and is presented in Table 4. The applicability of this model depends on the nature of the plot. The plot should be a straight line for the occurrence of intraparticle diffusion. In this study, multilinearity can be seen through Fig. S5. k_{id} and intercept were found as 2.34 and 9.56 respectively. The graph shows the involvement of 3 steps: The first step occurred between 10 and 40 min and yielded a straight line ($R^2 = 0.99$) with k_{id1} and C_1 values of 0.68 and 17.69 respectively. This marked the occurrence of film diffusion in the first step through

Fig. 10 Nonlinear fitting of pseudo-first-order and pseudo-second-order kinetic for As(V) adsorption on FeBPB

Table 4 Kinetic model parameters for As(V) removal by FeBPB

Pseudo first order	
k_1 (1/min)	0.0365
q_e(T) (µg/g)	34.54
q_e(E) (µg/g)	40
R^2	0.50
χ^2	0.74
S.S.E	29.81
Pseudo second order	
k_2 (g µg^{-1} min^{-1})	19.41×10^{-2}
q_e(T) (µg/g)	39.60
q_e(E) (µg/g)	40
R^2	0.67
χ^2	0.004
S.S.E	0.16
Intra particular diffusion	
k_{id} (µgg^{-1} min$^{-0.5}$)	2.34
Intercept	9.56
R^2	0.91

which the adsorption took place. Similarly, the second and third step yielded relatively smaller values of intercept (2.72 and 0.825) which evince the existence of intraparticle diffusion in the later stage of removal. Thus, it was concluded that As(V) adsorption using FeBPB was solely not controlled by intraparticle diffusion.

Thermodynamic study

Apart from isotherm and kinetic studies, adsorption mechanism was additionally complemented by the estimation of thermodynamic parameters. Thermodynamic studies were carried out by using the data of temperature-related experiments. The parameters such as standard free energy (ΔG^o), standard enthalpy (ΔH^o), and standard entropy (ΔS^o) were found using the following equations (Eqs. (11) and (12)) (Dehghani et al. 2018b; Rodrigues et al. 2018).

$$\Delta G^0 = -RT \ln K_C \quad (11)$$

$$\ln K_c = \frac{\Delta S^0}{R} - \frac{\Delta H^0}{RT} \quad (12)$$

It is noteworthy to point out that the determination of thermodynamic parameters is greatly affected by the thermodynamic equilibrium constant (K_c). For correct estimation of parameters, K_c should be dimensionless (Milonjić 2007). K_c can be estimated by using Langmuir constant (K_L) for the diluted solution, which has charged adsorbate (Liu 2009). Since, Langmuir isotherm was the best performing model, so constant K_L was used for estimation of K_c. The unit of K_L (L/μg) was converted into liters per mole by multiplying the molar mass of arsenic (74.92 × 10^6 μg/mol). Further, K_L in liters per mole was multiplied by the density of water in moles per liter (55.56). ΔG° values at different temperatures were determined using Eq. (11). Similarly, ΔH° and ΔS° were obtained using Eq. (12) by plotting the data of ln K_c vs 1/T (Fig. S6). Results of the isotherm parameters are reported in Table 5. The adsorption was spontaneous as the ΔG° values were observed as − 46.88, − 48.58, and − 50.73 kJ/mol at 298, 308, and 318 correspondingly. Increase in negative value of ΔG° indicated that adsorption was favored at a lower temperature. Negative standard enthalpy (ΔH°) (− 10.55 kJ/mol) value indicates the exothermic characteristic of adsorption of As(V) on FeBPB, which is in good agreement with experimental observation. The exothermic behavior also confirmed the involvement of electrostatic interaction between FeBPB and As(V). The value

Table 5 Thermodynamic parameters for As(V) adsorption on FeBPB

T (K)	ΔG° (kJ/mol)	ΔH° (kJ/mol)	ΔS° (kJ/mol K)
298	− 46.88	− 10.55	0.123
308	− 48.58		
318	− 50.73		

of ΔS° was found as 0.123 kJ/mol·K. The positive value entails about the increase in entropy of the system. The results of experimental observation, characterization studies, and calculated parametric values of isotherm, kinetic, and thermodynamic equations complemented each other and confirmed that As(V) was being removed through electrostatic attraction and surface complexation.

Competing ions

The decrease in percentage removal of As(V) was detected when the concentration of the competing ions increased in As(V) spiked water (Fig. 11). Among the studied competing ions, nitrate had comparatively less impact on As(V) removal, but phosphate was found to be strong competitors of arsenic for adsorption sites. The overall order of increasing effect on As(V) removal of the competing ions was nitrate < sulfate < silicate < phosphate. Phosphate and silicate were found a strong competitor for As(V) adsorption sites. This is due to the fact that as similar to As(V), in water, phosphate, and silicate also form tetrahedral oxyanions (Ghosh et al. 2019). Species in polymeric form cover more of the FeBPB surface and adsorption sites than its monomeric form, thereby hindering of adsorption of As(V) by steric effects or through decreasing the surface potential (Tuutijärvi et al. 2012).

Possible mechanisms of As(V) adsorption onto FeBPB

Considering the results of experimental investigations of isotherm, kinetic, pH, and thermodynamic studies along with the characterization of FeBPB, following possible mechanism can be put forward for arsenic adsorption. FTIR spectra clearly showed that there was plenty of oxygen-containing functional group, which took part in the binding of the arsenate ions. Characterization studies also confirmed that adsorption of As(V) occurred due to the presence of iron in the form of hydroxide and arsenic in the form of As(V) and during the
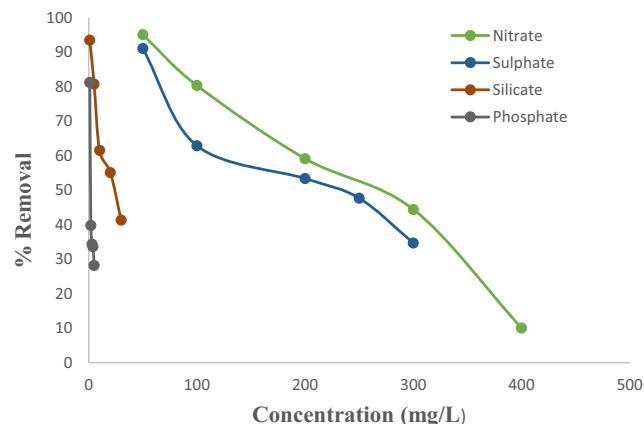

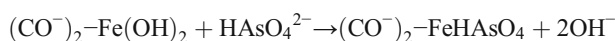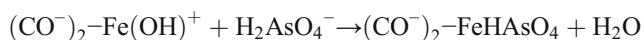**Fig. 11** Effect of competing ions on As(V) removal using FeBPB

Table 6 Model summary of MLR analysis

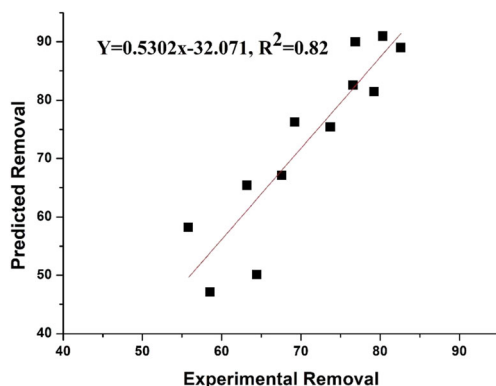| Model	Unstandardized coefficients		Standardized coefficients	t	Sig.	95.0% confidence interval for B	
	B	Std. Error	Beta			Lower bound	Upper bound
(Constant)	49.463	18.319		2.700	0.010	12.543	86.383
Time	0.185	0.040	0.421	4.617	0.000	0.104	0.265
Conc	− 0.060	0.016	− 0.393	− 3.786	0.000	− 0.092	− 0.028
Dose	12.105	2.453	0.453	4.934	0.000	7.161	17.050
pH	− 3.456	1.967	− 0.160	− 1.757	0.086	− 7.420	0.508
Temp	0.137	0.299	0.048	0.460	0.648	− 0.464	0.739

adsorption, there was no conversion of As(V) into As(III). The surface of bio adsorbents predominantly had C–OH surface hydroxy groups (Corapcioglu and Huang 1987; Manju et al. 1998; Hu et al. 2015). The interaction of iron on the surface of banana pith biochar can be described using the following relation.

$$2COH + Fe(OH)^+ \rightarrow (CO^-)_2{-}FeOH^+ + 2H^+$$

$$2COH + Fe(OH)_2 \rightarrow (CO^-)_2{-}Fe(OH)_2 + 2H^+$$
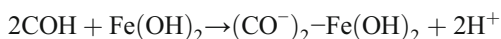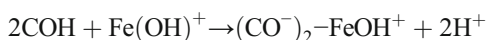
Generally, the arsenic adsorption is governed by two factors, i.e., arsenic speciation and surface charge of adsorbent. It has already been reported that As(V) occurs in solution in the form of H_3AsO_4, $H_2AsO_4^-$, $HAsO_4^{2-}$, and AsO_4^{3-} oxyanions at pH < 2, pH 2–7, pH 7–11, and pH 11–14 respectively. In drinking water pH range, $H_2AsO_4^-$ and $HAsO_4^{2-}$ are the major As(V) oxyanions (Smedley and Kinniburgh 2002). Therefore, these were predominantly positively charged under experimental condition. Possible electrostatic interaction with these two species is discussed below.

$$(CO^-)_2{-}Fe(OH)^+ + H_2AsO_4^- \rightarrow (CO^-)_2{-}FeHAsO_4 + H_2O$$

$$(CO^-)_2{-}Fe(OH)_2 + HAsO_4^{2-} \rightarrow (CO^-)_2{-}FeHAsO_4 + 2OH^-$$

Another possible mechanism may be interaction of As(V) species ($H_2AsO_4^-$ and $HAsO_4^{2-}$) with iron oxy-hydroxides.

This iron oxy-hydroxides can be protonated or deprotonated depending on the pH value of solutions (Pehlivan et al. 2013).

$$Fe{-}OH + H^+ \rightarrow Fe(OH)_2^+$$

$$Fe{-}OH \rightarrow H^+ + FeO^-$$
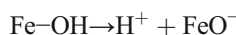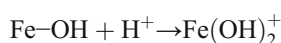
Adsorption of $H_2AsO_4^-$ on FeBPB surface when iron is in protonated iron hydroxide form occurred due to the formation of surface complexes and coulombic attraction.

$$FeOH_2^+ + H_2AsO_4^- \rightarrow [Fe{-}(O)_2{-}AsO(OH)]^- + H_3O^+$$

$$FeOH_2^+ + H_2AsO_4^- \rightarrow FeOH^+ \dots {}^-O_4AsH_2$$
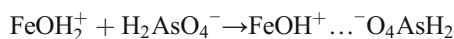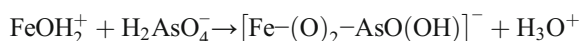
Adsorption of $H_2AsO_4^-$ (pH 2–7) and $HAsO_4^{2-}$ (pH > 7) might also be occurred due to ligand exchange but this type of adsorption will not be much effective because increase in negative ions in solution reduces As(V) removal.

$$Fe{-}OH + H_2AsO_4^- \rightarrow Fe{-}OAsO_3H_2 + OH^-$$

$$Fe{-}OH + HAsO_4^{2-} \rightarrow FeOAsO_3H^- + OH^-$$
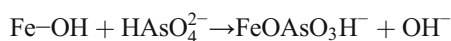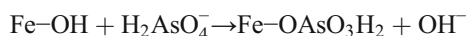
XRD results showed that there was no new peak of crystalline phase of adsorbed arsenic. Adsorbed arsenic did not affect the crystal structure of iron, which confirmed the absence of precipitate phase. However, it is worth noting that arsenic-bounded FeBPB was amorphous in phase; also, there might not be enough arsenic on the surface which could have been detected through XRD. With the present results, the occurrence of precipitation can be ruled out. Similar findings have been given by the Hu and co-workers (Hu et al. 2015). In the present study, adsorption was supposedly occurred through binding with functional groups, electrostatic attraction, and surface complexation.

Prediction modeling

Experimental observations were analyzed to develop a regression equation. Using the developed equation, the amount of removal efficiencies can be predicted without conducting any removal experiments in advance. The coefficient values

Fig. 12 Correlation between model predicted and experimental removal of As(V) on FeBPB

Y=0.5302x-32.071, R²=0.82

obtained during analysis are presented in Table 5 and these were used to generate the following regression equation.

$$\text{Removal} = 49.463 + 0.185\ \text{Time} - 0.060\ \text{Conc.}$$
$$+ 12.10\ \text{Dose} - 3.456\ \text{pH} + 0.137\ \text{Temp.} \quad (13)$$

It is seen from Table 6 that FeBPB dose with the highest coefficient value has a substantial effect on removal efficiency. It was perceived that except pH and temperature, all other parameters had significance ($p < 0.05$). It shows that time, concentration, and dose were found statistically significant in MLR analysis. It is noteworthy to mention that other remaining parameters may not have statistical significance, but it is practically signified, as noted during adsorption experiments. Results of model validation using different data sets are presented in Fig. 12. The high R^2 value of 0.82 was found between experimental removal efficiency and MLR predicted removal efficiency. It reveals that as per the model, independent variables like concentration, time, dose, pH, and temperature accounted for 82% of the total variability of removal efficiency.

Conclusions

This study demonstrated the utilization of agricultural waste (banana pith) as a value-added product for arsenic remediation in aqueous solutions. Further, synthesizing iron-loaded biochar gave the synergistic effect for As(V) removal. Prepared FeBPB composite exhibited good surface properties like fine pore structure, more oxygen-containing functional groups, and high surface area, which facilitated an easy As(V) removal. XPS analysis revealed that the arsenic was adsorbed as As(V) only and there was no conversion of As(V) into As(III). Adsorption isotherm was sufficiently explained by Langmuir isotherm with a maximum monolayer adsorption capacity of 120.91 μg/g at 298 K. Kinetics of removal process was better explained by pseudo-second-order kinetic model. Except for phosphate, other coexisting anions showed insignificant effects on As(V) removal by the FeBPB. High pHzpc value (9.5) provided added advantage of excellent removal up to pH 7.5. More importantly, there was no variation in pH after the adsorption process, which made this adsorbent a viable and economical candidate for arsenic remediation purposes. MLR prediction modeling showed that all the independent variables were accounted for 82% of the variation in removal efficiency and the generated model equation can be applied to simulate the removal pattern for any variation in the affecting parameters.

References

Ali I, Al-Othman ZA, Alwarthan A, Asim M, Khan TA (2014) Removal of arsenic species from water by batch and column operations on bagasse fly ash. Environ Sci Pollut Res 21(5):3218–3229

Allen SJ, Mckay G, Porter JF (2004) Adsorption isotherm models for basic dye adsorption by peat in single and binary component systems. J Colloid Interface Sci 280(2):322–333

Carlin DJ, Naujokas MF, Bradham KD, Cowden J, Heacock M, Henry HF, Waalkes MP (2015) Arsenic and environmental health: state of the science and future research opportunities. Environ Health Perspect 124(7):890–899

Cope CO, Webster DS, Sabatini DA (2014) Arsenate adsorption onto iron oxide amended rice husk char. Sci Total Environ 488–489:554–561

Corapcioglu MO, Huang CP (1987) The adsorption of heavy metals onto hydrous activated carbon. Water Res 21(9):1031–1044

Crittenden JC, Harza BMW (2005) Water treatment: principles and design. Wiley

Dehghani MH, Zarei A, Mesdaghinia A, Nabizadeh R, Alimohammadi M, Afsharnia M (2017a) Response surface modeling, isotherm, thermodynamic and optimization study of arsenic (V) removal from aqueous solutions using modified bentonite-chitosan (MBC). Korean J Chem Eng 34(3):757–767

Dehghani MH, Zarei A, Mesdaghinia A, Nabizadeh R, Alimohammadi M, Afsharnia M (2017b) Adsorption of Cr (VI) ions from aqueous systems using thermally sodium organo-bentonite biopolymer composite (TSOBC): response surface methodology, isotherm, kinetic and thermodynamic studies. Desalin Water Treat 85:298–312

Dehghani MH, Tajik S, Panahi A, Khezri M, Zarei A, Heidarinejad Z, Yousefi M (2018a) Adsorptive removal of noxious cadmium from aqueous solutions using poly urea-formaldehyde: a novel polymer adsorbent. MethodsX 5:1148–1155

Dehghani MH, Zarei A, Mesdaghinia A, Nabizadeh R, Alimohammadi M, Afsharnia M, McKay G (2018b) Production and application of a treated bentonite–chitosan composite for the efficient removal of humic acid from aqueous solution. Chem Eng Res Des 140:102–115

Ebrahimi R, Maleki A, Shahmoradi B, Daraei H, Mahvi AH, Barati AH, Eslami A (2013) Elimination of arsenic contamination from water using chemically modified wheat straw. Desalin Water Treat 51(10-12):2306–2316

Ghosh S, Prabhakar R, Samadder SR (2019) Performance of γ-aluminium oxide nanoparticles for arsenic removal from groundwater. Clean Techn Environ Policy 21(1):121–138

Hering JG, Chen PY, Wilkie JA, Elimelech M, Liang S (1996) Arsenic removal by ferric chloride. J Am Water Works Assoc 88(4):155–167

Ho YS (1995) Absorption of heavy metals from waste streams by peat (Doctoral dissertation, University of Birmingham)

Hu X, Ding Z, Zimmerman AR, Wang S, Gao B (2015) Batch and column sorption of arsenic onto iron-impregnated biochar synthesized through hydrolysis. Water Res 68:206–216

Hughes MF, Del Razo LM, Kenyon EM (2000) Dose-dependent effects on tissue distribution and metabolism of dimethylarsinic acid in the mouse after intravenous administration. Toxicology 143(2):155–166

Jia YF, Xu LY, Wang X, Demopoulos GP (2007) Infrared spectroscopic and X-ray diffraction characterization of the nature of adsorbed arsenate on ferrihydrite. Geochim Cosmochim Acta 71(7):1643–1654

Khan TA, Chaudhry SA, Ali I (2013) Thermodynamic and kinetic studies of As(V) removal from water by zirconium oxide-coated marine sand. Environ Sci Pollut Res 20(8):5425–5440

Khosravi R, Eslami H, Zarei A, Heidari M, Baghani AN, Safavi N, Adhami S (2018) Comparative evaluation of nitrate adsorption from aqueous solutions using green and red local montmorillonite adsorbents. Desalin Water Treat 116:119–128

Kumar A, Samadder SR (2017) An empirical model for prediction of household solid waste generation rate–a case study of Dhanbad, India. Waste Manag 68:3–15

Lagergren SK (1898) About the theory of so-called adsorption of soluble substances. Sven Vetenskapsakad Handingarl 24:1–39

Lata S, Samadder SR (2016) Removal of arsenic from water using nano adsorbents and challenges: a review. J Environ Manag 166:387–406

Liu Y (2009) Is the free energy change of adsorption correctly calculated? J Chem Eng Data 54(7):1981–1985

Liu S, Xu WH, Liu YG, Tan XF, Zeng GM, Li X, Cai XX (2017) Facile synthesis of Cu (II) impregnated biochar with enhanced adsorption activity for the removal of doxycycline hydrochloride from water. Sci Total Environ 592:546–553

Manju GN, Raji C, Anirudhan TS (1998) Evaluation of coconut husk carbon for the removal of arsenic from water. Water Res 32(10):3062–3070

Milonjić SK (2007) A consideration of the correct calculation of thermodynamic parameters of adsorption. J Serb Chem Soc 72(12):1363–1367

Mishra T, Mahato DK (2016) A comparative study on enhanced arsenic (V) and arsenic (III) removal by iron oxide and manganese oxide pillared clays from ground water. J Environ Chem Eng 4(1):1224–1230

Mohan D, Pittman CU Jr (2007) Arsenic removal from water/wastewater using adsorbents—a critical review. J Hazard Mater 142(1-2):1–53

Mohan D, Sharma R, Singh VK, Steele P, Pittman CU Jr (2012) Fluoride removal from water using bio-char, a green waste, low-cost adsorbent: equilibrium uptake and sorption dynamics modeling. Ind Eng Chem Res 51(2):900–914

Mohan D, Sarswat A, Ok YS, Pittman CU Jr (2014) Organic and inorganic contaminants removal from water with biochar, a renewable, low cost and sustainable adsorbent–a critical review. Bioresour Technol 160:191–202

Montero JIZ, Monteiro AS, Gontijo ES, Bueno CC, de Moraes MA, Rosa AH (2018) High efficiency removal of As (III) from waters using a new and friendly adsorbent based on sugarcane bagasse and corncob husk Fe-coated biochars. Ecotoxicol Environ Saf 162:616–624

Mudhoo A, Sharma SK, Garg VK, Tseng CH (2011) Arsenic: an overview of applications, health, and environmental concerns and removal processes. Crit Rev Environ Sci Technol 41(5):435–519

Mukherjee A, Zimmerman AR, Harris W (2011) Surface chemistry variations among a series of laboratory-produced biochars. Geoderma 163(3-4):247–255

Patra AK, Dutta A, Bhaumik A (2012) Self-assembled mesoporous γ-Al2O3 spherical nanoparticles and their efficiency for the removal of arsenic from water. J Hazard Mater 201:170–177

Pehlivan E, Tran TH, Ouédraogo WKI, Schmidt C, Zachmann D, Bahadir M (2013) Removal of As (V) from aqueous solutions by iron coated rice husk. Fuel Process Technol 106:511–517

Pintor AM, Vieira BR, Santos SC, Boaventura RA, Botelho CM (2018) Arsenate and arsenite adsorption onto iron-coated cork granules. Sci Total Environ 642:1075–1089

Prabhakar R, Samadder SR (2018) Low cost and easy synthesis of aluminium oxide nanoparticles for arsenite removal from groundwater: a complete batch study. J Mol Liq 250:192–201

Qasemi M, Shams M, Sajjadi SA, Farhang M, Erfanpoor S, Yousefi M, Afsharnia M (2019) Cadmium in groundwater consumed in the rural areas of Gonabad and Bajestan, Iran: occurrence and health risk assessment. Biol Trace Elem Res:1–10

Randhawa NS, Murmu N, Tudu S, Sau DC (2014) Iron oxide waste to clean arsenic-contaminated water. Environ Chem Lett 12(4):517–522

Rizwan M, Ali S, Qayyum MF, Ibrahim M, Zia-ur-Rehman M, Abbas T, Ok YS (2016) Mechanisms of biochar-mediated alleviation of toxicity of trace elements in plants: a critical review. Environ Sci Pollut Res 23(3):2230–2248

Rodrigues DA, Moura JM, Dotto GL, Cadaval TR, Pinto LA (2018) Preparation, characterization and dye adsorption/reuse of chitosan-vanadate films. J Polym Environ 26(7):2917–2924

Roy PK, Majumder A, Banerjee G, Roy MB, Pal S, Mazumdar A (2015) Removal of arsenic from drinking water using dual treatment process. Clean Techn Environ Policy 17(4):1065–1076

Samiey B, Cheng C, Wu J (2014) Organic-inorganic hybrid polymers as adsorbents for removal of heavy metal ions from solutions: a review. J Mater 7:673–726

Siddiqui SI, Chaudhry SA (2017) Iron oxide and its modified forms as an adsorbent for arsenic removal: a comprehensive recent advancement. Process Saf Environ Prot 111:592–626

Smedley PL, Kinniburgh DG (2002) A review of the source, behavior and distribution of arsenic in natural waters. Appl Geochem 17:517–568

Sorlini S, Gialdini F (2010) Conventional oxidation treatments for the removal of arsenic with chlorine dioxide, hypochlorite, potassium permanganate and monochloramine. Water Res 44(19):5653–5659

Tan XF, Liu YG, Gu YL, Xu Y, Zeng GM, Hu XJ, Li J (2016) Biochar-based nano-composites for the decontamination of wastewater: a review. Bioresour Technol 212:318–333

Tang J, Zhu W, Kookana R, Katayama A (2013) Characteristics of biochar and its application in remediation of contaminated soil. J Biosci Bioeng 116(6):653–659

Thanh DN, Bastl Z, Černá K, Ulbrich P, Lederer J (2016) Amorphous nanosized Al–Ti–Mn trimetal hydrous oxides: synthesis, characterization and enhanced performance in arsenic removal. RSC Adv 6(103):100732–100742

Tuutijärvi T, Repo E, Vahala R, Sillanpää M, Chen G (2012) Effect of competing anions on arsenate adsorption onto maghemite nanoparticles. Chin J Chem Eng 20(3):505–514

Vázquez G, Mosquera O, Freire MS, Antorrena G, González-Álvarez J (2012) Alkaline pre-treatment of waste chestnut shell from a food industry to enhance cadmium, copper, lead and zinc ions removal. Chem Eng J 184:147–155

Velazquez-Jimenez LH, Arcibar-Orozco JA, Rangel-Mendez JR (2018) Overview of As (V) adsorption on Zr-functionalized activated carbon for aqueous streams remediation. J Environ Manag 212:121–130

Vindedahl AM, Strehlau JH, Arnold WA, Penn RL (2016) Organic matter and iron oxide nanoparticles: aggregation, interactions, and reactivity. Environ Sci Nano 3(3):494–505

Weber WJ, Morris JC (1963) Kinetics of adsorption on carbon from solution. J Sanit Eng Div 89(2):31–60

WHO/UNICEF Joint Water Supply, & Sanitation Monitoring Programme (2014) Progress on drinking water and sanitation: 2014 Update. World Health Organization

Yonesian M, Mahvi AH, Ali Mohammadi M, Dehghani MH, Nazmara S (2012) Cadmium, lead and arsenic concentration in soil and underground water and its relationship with chemical fertilizer in paddy soil. J Mazandaran Univ Med Sci 21(1):20–28

Zhang MM, Liu YG, Li TT, Xu WH, Zheng BH, Tan XF, Wang SF (2015) Chitosan modification of magnetic biochar produced from Eichhornia crassipes for enhanced sorption of Cr (VI) from aqueous solution. RSC Adv 5(58):46955–46964

Zhou Z, Liu YG, Liu SB, Liu HY, Zeng GM, Tan XF, Cai XX (2017) Sorption performance and mechanisms of arsenic (V) removal by magnetic gelatin-modified biochar. Chem Eng J 314:223–231